

Soliton Microcombs Multiplexing Using Intracavity-Stimulated Brillouin LasersHao Zhang,¹ Teng Tan,¹ Hao-Jing Chen^{2,3}, Yan Yu,^{2,3} Wenting Wang,⁴ Bing Chang,¹ Yupei Liang,¹
Yanhong Guo,¹ Heng Zhou,¹ Handing Xia,⁵ Qihuang Gong,² Chee Wei Wong⁴,Yunjiang Rao,^{1,6,*} Yun-Feng Xiao,^{2,†} and Baicheng Yao^{1,‡}¹*Key Laboratory of Optical Fibre Sensing and Communications (Education Ministry of China),
University of Electronic Science and Technology of China, Chengdu 611731, China*²*State Key Laboratory for Mesoscopic Physics and Frontiers Science Center for Nano-optoelectronics,
School of Physics, Peking University, Beijing 100871, China*³*T. J. Watson Laboratory of Applied Physics, California Institute of Technology, Pasadena, California 91125, USA*⁴*Fang Lu Mesoscopic Optics and Quantum Electronics Laboratory, University of California,
Los Angeles, California 90095, USA*⁵*Research Center of Laser Fusion, China Academic of Engineering Physics, Mianyang 621900, China*⁶*Research Centre for Optical Fiber Sensing, Zhejiang Laboratory, Hangzhou 310000, China*

(Received 16 August 2022; accepted 17 March 2023; published 12 April 2023)

Solitons in microresonators have spurred intriguing nonlinear optical physics and photonic applications. Here, by combining Kerr and Brillouin nonlinearities in an over-modal microcavity, we demonstrate spatial multiplexing of soliton microcombs under a single external laser pumping operation. This demonstration offers an ideal scheme to realize highly coherent dual-comb sources in a compact, low-cost and energy-efficient manner, with uniquely low beating noise. Moreover, by selecting the dual-comb modes, the repetition rate difference of a dual-comb pair could be flexibly switched, ranging from 8.5 to 212 MHz. Beyond dual-comb, the high-density mode geometry allows the cascaded Brillouin lasers, driving the co-generation of up to 5 space-multiplexing frequency combs in distinct mode families. This Letter offers a novel physics paradigm for comb interferometry and provides a widely appropriate tool for versatile applications such as comb metrology, spectroscopy, and ranging.

DOI: [10.1103/PhysRevLett.130.153802](https://doi.org/10.1103/PhysRevLett.130.153802)

Owing to the high quality (Q) factor and small mode volume, light-matter interaction is dramatically enhanced in optical microresonators, which makes them become a captivating platform for nonlinear optical physics and photonic applications [1,2]. In particular, the microcavity-enhanced Kerr effect has led to the realization of frequency combs in a miniature platform [3–5]. In recent years, the blooming of soliton microcomb technology [6–10] has enabled versatile out-of-lab advances in applications ranging from optical communications [11–13], optical atomic clock [14,15], optical sensing [16], to dual-comb spectroscopy [17,18]. Especially, microcomb multiplexing methods are particularly appealing for applications such as dual-microcomb spectroscopy and LiDAR [19–22]. However, commonly these methods require either an additional external laser [23] or a fast electro-optic modulator [24] to obtain a second pump light for dual-soliton microcomb generation. The complexity and cost associated with the operation of multiple narrow-linewidth laser or high-bandwidth modulator devices limit the simplicity of the system and the mutual coherence between the comb outputs.

Stimulated Brillouin scattering (SBS), a process that arises from the coherent coupling between optical fields and phonons, is another intriguing nonlinear effect in

microcavities [25]. Resulting from its highly effective gain and narrow band features, the SBS process in microresonators has been used to generate intracavity ultra-narrow linewidth laser and further led to versatile applications in low-noise microwave signal generation [26], Brillouin gyroscope [27], and soliton generation [28].

Here, we demonstrate the spatial multiplexing of Kerr soliton microcombs in a single over-modal microresonator using intracavity Brillouin excitations. The intracavity Brillouin lasing not only provides pumping for an additional set of microcomb with naturally narrow linewidths and fixed phase relations to the primary pump light, which enables remarkably high coherence of the dual-comb source; but also eliminates the requirement for additional lasers or modulators, which can significantly simplify the dual-comb system. In such a high- Q silica microcavity supporting rich mode families, besides its own Kerr soliton formation, the pump laser can excite backwardly circulating cascaded Brillouin lasers (BLs) [29–31], when the Brillouin gain regions overlap varied resonances. By carefully controlling the pump laser detuning, these BLs can further work as “new pumps” for generating more soliton microcombs in diverse mode families. This scheme raises a new physical paradigm for soliton multiplexing, and offers

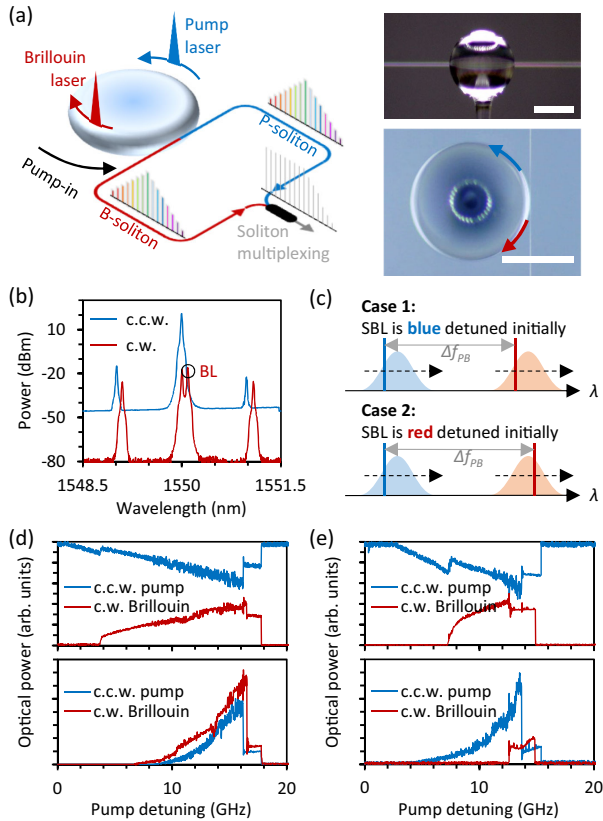


FIG. 1. Conceptual design of the counterpropagating dual soliton. (a) Schematic and micrograph of the microresonator and dual-comb generation. Scale bar: 300 μm . (b) Zoom-in spectrum of the CCW (blue) and CW (red) comb outputs. (c) Two cases of dual-comb generation. (d) and (e) The evolution of the two cases. The top panels show laser power traces while the bottom panels show comb power traces. Blue: CCW, red: CW.

a convenient way to realize dual-comb tools. Moreover, since both the Brillouin lasing [26,28] and the soliton formation are coherently realized in one single cavity, common mode noises are efficiently suppressed [32]. Furthermore, by selecting the excitation mode families of the dual comb, we demonstrate that the repetition rate difference of the generated dual comb could be flexibly switched, ranging from 8.5 to 212 MHz. Finally, owing to the over-modal cavity nature, the BL generation could be cascaded. Therefore, cogeneration of up to 5 spatial-multiplexing soliton frequency combs in distinct mode families is realized.

We utilize the over-modal nature with strong Brillouin scattering of a silica whispering-gallery-mode (WGM) cavity, as Fig. 1(a) shows. The microsphere is fabricated from a commercial optical fiber section using the discharge-sintering technique (Supplemental Material [33], Sec. I) with a diameter of $\sim 600 \mu\text{m}$ and a Q factor of 1.2×10^8 . A tunable external laser (pump laser, PL) is coupled into the cavity via a tapered fiber, circulating in the counterclockwise (CCW) direction. By properly tuning the PL frequency into a cavity resonance, stimulated BL could be generated in

the clockwise (CW) direction. Since the free spectral range (FSR) of our cavity is ~ 110 GHz while the Brillouin shift frequency is of the order of 10 GHz, the PL and the BL are usually located in two distinct mode families. In order to generate Brillouin-Kerr dual-comb, both mode families should exhibit anomalous group velocity dispersion (GVD). When further tuning the PL frequency from blue to red, we achieve single Kerr soliton state in both directions. The coexistence of such Brillouin-Kerr dual soliton is also demonstrated in numerical simulations (see Supplemental Material [33] Sec. III). The PL- and BL-based soliton have different repetition rates, and are easily combined via a fiber coupler to form dual-comb outputs.

The comb signals are collected in both CW and CCW directions, the enlarged spectra around the pump wavelength are shown in Fig. 1(b). The PL and the BL have a wavelength difference of 0.084 nm, which corresponds to the Brillouin shift frequency in silica and suggests the PL and BL belong to different spatial modes. Besides, the first pair of comb lines in the CCW and CW directions also have different wavelengths, verifying that the counterpropagating combs are generated by the PL and the BL, respectively. The process of dual-soliton co-generation is also investigated, and there are two different cases when scanning the PL across different modes [Fig. 1(c)]. The reason is that the initial “Brillouin gain–resonance” overlapping could be varied, while the frequency difference between the PL and the BL (Δf_{PB}) is typically fixed, determined by the material and the cavity geometry. In case 1, the BL is initially generated at the blue-detuned side of the BL mode, and the comb in both directions evolves regularly (i.e., from primary, chaotic, to soliton state in sequence), as shown in Fig. 1(d). While in case 2, the BL is initially generated at the red-detuned (or slightly blue-detuned) region. With the pump laser scanning, the power of the BL gradually increases. Once reaching the Kerr parametric oscillation threshold, soliton burst is triggered [39], as shown in Fig. 1(e). In this measurement, the PL scanning speed is 50 GHz/s and the PL power is fixed at 120 mW. Thanks to the high- Q factor of the cavity and the self-stabilization of the BL [40], the experimentally obtained soliton step existence range reaches 2 GHz. It is noted that the phenomenon of “pump + Brillouin” dual-soliton co-generation is not certain for every mode pair, as the Brillouin gain band may not cover a high- Q resonance with anomalous dispersion.

The co-generated PL-based CCW soliton and the BL-based CW soliton are characterized after generation. The optical spectra are shown in Fig. 2(a). In these two spectra, power of the PL is lower than the BL due to the pump filtering operation. For the steady state shown here, $\Delta f_{PB} \approx 10.48$ GHz. The soliton spectra are broad, with 3 dB bandwidths of 1.47 and 0.95 THz. Spectrum of the BL-based soliton slightly deviates from the sech^2 shape, which may result from higher order dispersion in the BL

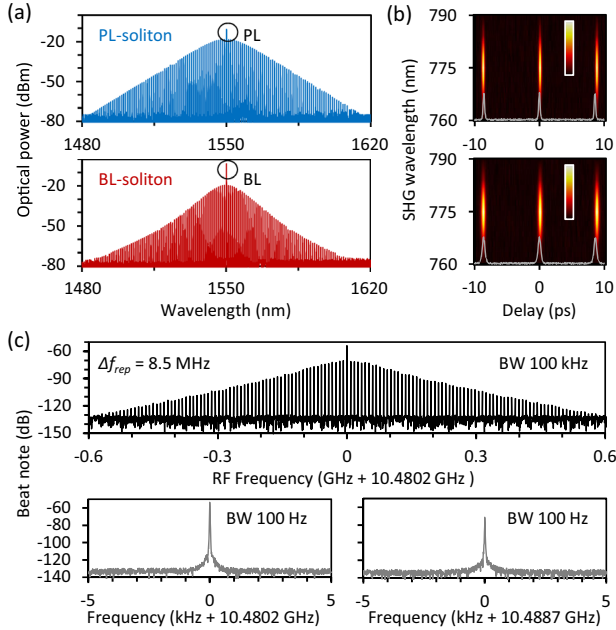


FIG. 2. The co-generated dual soliton. (a) Optical spectra, top and bottom panels: PL- and BL-generated single soliton. (b) FROG maps corresponding to (a). Grey curves show the autocorrelation traces of the two pulse trains. Color bar: normalized pulse intensity. (c) Top panel: Dual-soliton beat note in the rf domain. Central frequency of the electrical comb is 10.4802 GHz, determined by Δf_{PB} . The electrical comb line spacing equals to $\Delta f_{rep} = 8.5$ MHz. Bottom panels show the enlarged spectra of the pump-Brillouin laser beat note (at 10.4802 GHz) and the first-order comb line pair beat note (at 10.4887 GHz).

mode family [41]. Using the second harmonic generation (SHG)-based autocorrelation technique, we also measured frequency-resolved-optical-gating (FROG) maps of the two soliton combs [Fig. 2(b)]. The retrieved pulse duration of the CCW and the CW soliton is 215 and 332 fs, respectively, matching their optical spectra well. Three soliton pulses are shown in a single FROG frame, with a temporal window of 20 ps. For the CCW soliton, the repetition period is 8.9532 ps, while for the CW soliton, the repetition period is 8.9539 ps, verifying the repetition frequency difference between the two combs.

After combining two solitons together, we measure the dual-comb beat notes in Fig. 2(c). Mixing of the two solitons forms an electrical comb in the radio frequency (rf) domain. The strongest central beat note locates at 10.4802 GHz (Δf_{PB}). This is the beat between the PL and the BL at mode number $\mu = 0$. On both sides of this beating line, other comb lines demonstrate the one-to-one beat notes between the two frequency combs. The spacing of the electrical comb is equal to the repetition frequency difference ($\Delta f_{rep} = 8.5$ MHz) between the two soliton combs. Since $\Delta f_{PB} \gg \Delta f_{rep}$, there is no spectral aliasing. By zooming the rf spectrum in, we characterize the two beat notes, at 10.4802 GHz

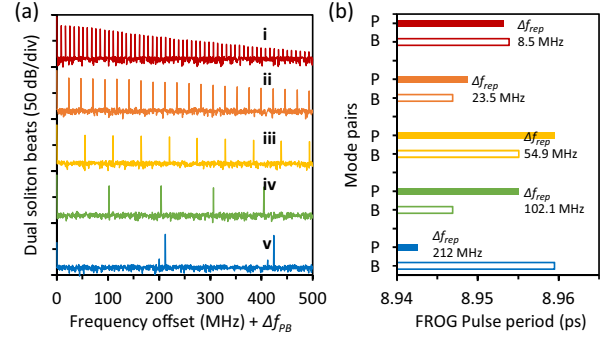


FIG. 3. Switchable dual-soliton beating. (a) Distinct dual-soliton beats when the PL and the BL locate in different modes. Here we only show the single sideband for better clarity. From top to bottom, Δf_{rep} increases from 8.5 to 212 MHz. (b) Measured pulse periods of the dual-soliton pairs. Here the solid and the hollow columns show the pulse periods of the PL-based soliton (P) and the BL-based (B), for case *i* to *v*.

($\mu = 0$, Δf_{PB}) and 10.4887 GHz ($\mu = 1$, $\Delta f_{PB} + \Delta f_{rep}$). Signal to noise ratio (SNR) of the pump-Brillouin beat is higher than 60 dB; meanwhile, SNR of the beat note between the first order comb line pairs is approaching 50 dB. Noise analyses are shown in the Supplemental Material [33], Sec. IV.

Since the over-modal microresonator has many co-existing mode families, such dual-comb multiplexing could appear in varied mode pairs. The group index of these mode families is different, offering chances to obtain distinct Δf_{rep} in dual-comb interference. This unique property enables varied dual-comb beat notes in a single microresonator. Experimentally, different mode pairs could be selected by carefully tuning the PL wavelength into a specific mode and exciting the BL in another specific mode. Figure 3(a) shows 5 distinct beat notes in the rf domain by exciting dual-soliton in varied mode pairs. From top to bottom, the PL wavelength is located at 1550.024, 1550.013, 1550.816, 1551.21, and 1550.72 nm. Δf_{rep} of the five cases are 8.5, 23.5, 54.9, 102.1, and 212 MHz, correspondingly. We also note that Δf_{rep} could be even higher, up to several GHz, but once Δf_{rep} is higher than 300 MHz, the limited Δf_{PB} may cause beat aliasing in the rf domain. Since the repetition rates and pulse periods are related to the group refractive index of the PL and BL mode, the specific PL-BL mode pair for the above 5 cases are varied. Δf_{rep} of the five cases are confirmed by the pulse periods obtained from the FROG measurements, as Fig. 3(b) shows. The pulse periods of the PL solitons are 8.9532, 8.9491, 8.9588, 8.9549, and 8.9423 ps; meanwhile the pulse periods of the BL solitons are 8.9539, 8.9473, 8.9549, 8.9468, and 8.9591 ps. We note that in our microsphere geometry supporting more than 100 transverse mode families, to accurately identify the specific mode-to-mode pairs is difficult, but high-density mode distribution

still offers a unique chance to find diverse dual-soliton combinations, which enables the Δf_{rep} of a dual-comb tool to be switchable.

This over-modal nature not only supports switchable dual-soliton beat notes, but also provides a possibility of cascaded BL generation if there are 3 or more resonances with a uniform spacing of ≈ 10.48 GHz and sufficiently high Q factors. Once all modes exhibit anomalous dispersion, > 2 soliton multiplexing can be realized in the single microresonator, by carefully selecting the pumping mode and combining the comb outputs from both the CW and the CCW directions. Such an operation further enriches the diversity of the microcomb device.

In the experiments, the multiplexed microcombs are collected from both the CW and CCW directions through a fiber coupler. The spectra around the pump laser wavelength are shown in Fig. 4(a). From top to bottom, we excite 1, 2, 3, and 4 BLs by carefully tuning the wavelength of a single PL. Each Brillouin excitation is driven by the optical signal ~ 10.48 GHz above it and belongs to a distinct mode family. These lasers travel in opposite directions one by one, for example, the PL propagates in the CCW direction, while the 1st, 2nd, 3rd, and 4th order BL go in CW, CCW, CW, and CCW directions, respectively. All the Brillouin lasers are capable of generating Kerr combs in principle. Figure 4(b) demonstrates the optical spectra of 2, 3, 4, and 5 Kerr comb multiplexing, from top to bottom. The rf spectrum of the comb states in the 0–400 MHz band is shown in Fig. 4(c). Among the four comb states, state *i*, *ii*, and *iv* feature low noise. Nevertheless, we do not claim that every comb here is in the single soliton state, because the mixed measurement of interferogram for 5 comb multiplexing needs > 40 GHz bandwidth in heterodyne characterization, and the mixed temporal trace of them is too complex to be well distinguished. For case *iii*, the rf noise is high, meaning there is at least one chaotic comb inside.

Taking advantage of the propagating direction difference of the intracavity frequency combs, we can easily measure the two-comb interferograms, by further down mixing the beat notes electrically using a 10 GHz sinusoidal signal. From top to bottom, Fig. 4(d) plots the temporal traces of several dual-comb pairs. Here the colored arrows present the comb circulating directions, corresponding to Fig. 4(a). For instance, in case *i*, both the CCW comb (driven by the PL) and the CW comb (driven by the first order BL) are in a single soliton state, temporal delay per round-trip of them is 117.65 ns ($\Delta f_{\text{rep}} = 8.5$ MHz, see Fig. 2), as the blue curve plots. In case *ii*, the CCW circulating comb driven by the PL is a single soliton, but there are four solitons in the CCW circulating comb driven by the second order BL, we see thus each cluster has 4 pulses in the down-mixed signal. In case *iii*, we know the CCW circulating comb driven by the PL is a single soliton (it appears first), and the copropagating dual-comb interference delivers equidistant pulse train

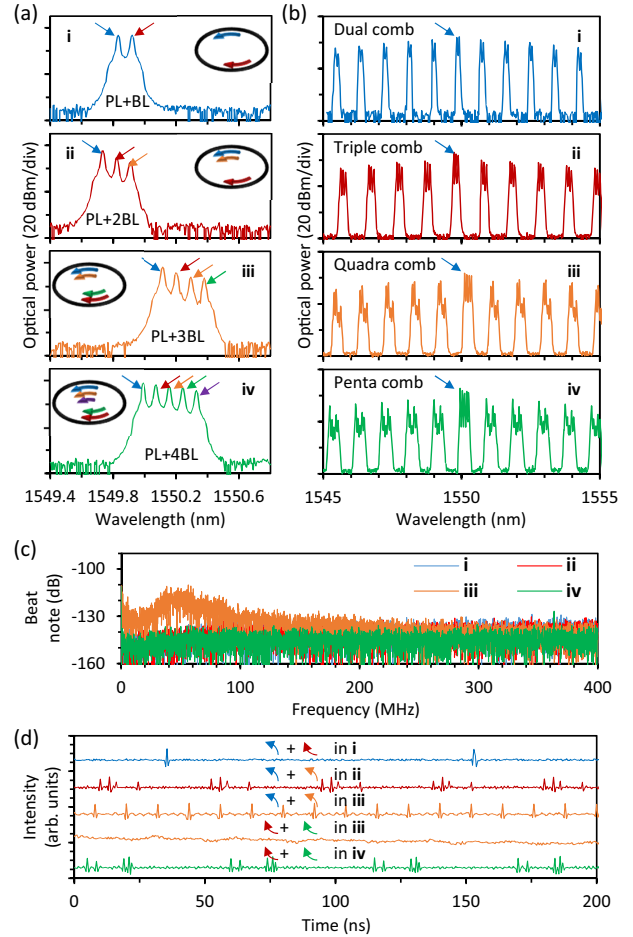


FIG. 4. Microcombs multiplexing using cascaded Brillouin lasers. (a) Single PL generates cascaded BLs in distinct mode families, from *i* to *iv*, up to 4 BLs are generated. Colored arrows: PL and cascaded BLs. (b) Co-excitation of multicomb in a single microresonator. From *i* to *iv*, in every bunch one can see 2–5 comb lines. The equally distributed line-to-line spacing is determined by the Δf_{PB} . (c) Measured rf spectrum (0–400 MHz) of case *i* to *iv*. (d) Dual-comb interferograms in case *i* to *iv*. In the dual-soliton heterodyne, stable pulse clusters demonstrate a stable Δf_{rep} .

(period 12 ns, $\Delta f_{\text{rep}} = 83.3$ MHz). We speculate that the comb generated by the 2nd BL is also a single soliton. On the other hand, the interferogram in the CW direction demonstrates chaotic features, suggesting that there is at least a noisy comb in the CW direction. Finally, in case *iv*, we observe 5 pulses in each cluster. The versatile dual-comb signal collected from either the “CW” or the “CCW” direction of such a multiplexed comb system offers a flexible tool for advanced applications such as optical frequency domain reflectometers [42,43] and vernier spectrometers [44,45].

In summary, by using a single PL and its stimulated BL excitations, *in situ* generation and spatial multiplexing of soliton microcombs in a single over-modal microresonator are demonstrated. Via tuning the PL frequency, both forwardly and backwardly circulating Kerr solitons could

be simultaneously excited. These two solitons have excellent mutual coherence, with an optical frequency offset of ~ 10.48 GHz, offering a scheme to realize dual comb interferometry conveniently. Careful mode selection enables the repetition rate difference of a dual-comb pair to be flexibly switchable, in a range of 8.5 to 212 MHz, experimentally. Moreover, we demonstrate that the BL generation could be cascaded, suggesting a way to co-generate up to 5 space-multiplexing frequency combs in varied mode families. This practically flexible and easily scalable method helps to improve our understanding about Brillouin-Kerr nonlinear interactions in microcavities, and inspires the simplification and integration of microcomb systems. It may show unique potential to extend the capabilities of microcomb interferometry based platforms in wide applications such as metrology, spectroscopy, and LiDAR.

We thank technical supports from Professor Qi-Fan Yang and Dr. Qi-Tao Cao at Peking University. We acknowledge financial support from the National Key Research and Development Program of China (2021YFB2800602), the National Natural Science Foundation of China (61975025, U2130106, 11825402, 11904339, and 12293051), the State Key laboratory (2022GZKF002), and the National Postdoctoral Innovation Talent Support Program of China (BX20220056).

H. Z., T. T., H.-J. C., Y. Y., and W. W. contributed equally to this work. B. Y. and Y.-F. X. led this study. H. Z., T. T., and W. W. contributed the experimental investigations, Y. Y. and H.-J. C. contributed the theoretical analysis. B. C., Y. L., Y. G., and H. X. built the experimental setup and fabricated the devices. All authors processed and analyzed the results. B. Y., Y. R., Y.-F. X., H.-J. C., and C. W. prepared the manuscript.

*Corresponding author.

yaobaicheng@uestc.edu.cn

†Corresponding author.

yjrao@uestc.edu.cn

‡Corresponding author.

yfxiao@pku.edu.cn

- [1] D. Armani, T. Kippenberg, S. Spillane, and K. Vahala, *Nature (London)* **421**, 925 (2003).
- [2] J. Liu, F. Bo, L. Chang, C.-H. Dong, X. Ou, B. Regan, X. Shen, Q. Song, B. Yao, W. Zhang *et al.*, *Sci. China Phys. Mech. Astron.* **65**, 1 (2022).
- [3] P. Del’Haye, A. Schliesser, O. Arcizet, T. Wilken, R. Holzwarth, and T. J. Kippenberg, *Nature (London)* **450**, 1214 (2007).
- [4] T. J. Kippenberg, R. Holzwarth, and S. A. Diddams, *Science* **332**, 555 (2011).
- [5] H.-J. Chen, Q.-X. Ji, H. Wang, Q.-F. Yang, Q.-T. Cao, Q. Gong, X. Yi, and Y.-F. Xiao, *Nat. Commun.* **11**, 2336 (2020).
- [6] T. Fortier and E. Baumann, *Commun. Phys.* **2**, 153 (2019).
- [7] B. Shen, L. Chang, J. Liu, H. Wang, Q.-F. Yang, C. Xiang, R. N. Wang, J. He, T. Liu, W. Xie *et al.*, *Nature (London)* **582**, 365 (2020).
- [8] C. Xiang, J. Liu, J. Guo, L. Chang, R. N. Wang, W. Weng, J. Peters, W. Xie, Z. Zhang, J. Riemensberger *et al.*, *Science* **373**, 99 (2021).
- [9] Z. Lu, H.-J. Chen, W. Wang, L. Yao, Y. Wang, Y. Yu, B. Little, S. Chu, Q. Gong, W. Zhao *et al.*, *Nat. Commun.* **12**, 3179 (2021).
- [10] L. Chang, S. Liu, and J. E. Bowers, *Nat. Photonics* **16**, 95 (2022).
- [11] P. Marin-Palomo, J. N. Kemal, M. Karpov, A. Kordts, J. Pfeifle, M. H. Pfeiffer, P. Trocha, S. Wolf, V. Brasch, M. H. Anderson *et al.*, *Nature (London)* **546**, 274 (2017).
- [12] B. Corcoran, M. Tan, X. Xu, A. Boes, J. Wu, T. G. Nguyen, S. T. Chu, B. E. Little, R. Morandotti, A. Mitchell *et al.*, *Nat. Commun.* **11**, 2568 (2020).
- [13] Y. Geng, H. Zhou, X. Han, W. Cui, Q. Zhang, B. Liu, G. Deng, Q. Zhou, and K. Qiu, *Nat. Commun.* **13**, 1070 (2022).
- [14] S. B. Papp, K. Beha, P. Del’Haye, F. Quinlan, H. Lee, K. J. Vahala, and S. A. Diddams, *Optica* **1**, 10 (2014).
- [15] Z. L. Newman, V. Maurice, T. Drake, J. R. Stone, T. C. Briles, D. T. Spencer, C. Fredrick, Q. Li, D. Westly, B. R. Ilic *et al.*, *Optica* **6**, 680 (2019).
- [16] T. Tan, Z. Yuan, H. Zhang, G. Yan, S. Zhou, N. An, B. Peng, G. Soavi, Y. Rao, and B. Yao, *Nat. Commun.* **12**, 6716 (2021).
- [17] I. Coddington, N. Newbury, and W. Swann, *Optica* **3**, 414 (2016).
- [18] N. Picqué and T. W. Hänsch, *Nat. Photonics* **13**, 146 (2019).
- [19] A. Dutt, C. Joshi, X. Ji, J. Cardenas, Y. Okawachi, K. Luke, A. L. Gaeta, and M. Lipson, *Sci. Adv.* **4**, e1701858 (2018).
- [20] M. Yu, Y. Okawachi, A. G. Griffith, N. Picqué, M. Lipson, and A. L. Gaeta, *Nat. Commun.* **9**, 1869 (2018).
- [21] P. Trocha, M. Karpov, D. Ganin, M. H. Pfeiffer, A. Kordts, S. Wolf, J. Krockenberger, P. Marin-Palomo, C. Weimann, S. Randel *et al.*, *Science* **359**, 887 (2018).
- [22] M.-G. Suh and K. J. Vahala, *Science* **359**, 884 (2018).
- [23] M.-G. Suh, Q.-F. Yang, K. Y. Yang, X. Yi, and K. J. Vahala, *Science* **354**, 600 (2016).
- [24] E. Lucas, G. Lihachev, R. Bouchand, N. G. Pavlov, A. S. Raja, M. Karpov, M. L. Gorodetsky, and T. J. Kippenberg, *Nat. Photonics* **12**, 699 (2018).
- [25] W. Loh, A. A. Green, F. N. Baynes, D. C. Cole, F. J. Quinlan, H. Lee, K. J. Vahala, S. B. Papp, and S. A. Diddams, *Optica* **2**, 225 (2015).
- [26] J. Li, H. Lee, and K. J. Vahala, *Nat. Commun.* **4**, 2097 (2013).
- [27] J. Li, M.-G. Suh, and K. Vahala, *Optica* **4**, 346 (2017).
- [28] Y. Bai, M. Zhang, Q. Shi, S. Ding, Y. Qin, Z. Xie, X. Jiang, and M. Xiao, *Phys. Rev. Lett.* **126**, 063901 (2021).
- [29] D. Braje, L. Hollberg, and S. Diddams, *Phys. Rev. Lett.* **102**, 193902 (2009).
- [30] K. Jia, X. Wang, D. Kwon, J. Wang, E. Tsao, H. Liu, X. Ni, J. Guo, M. Yang, X. Jiang *et al.*, *Phys. Rev. Lett.* **125**, 143902 (2020).
- [31] C. Qin, J. Du, T. Tan, B. Chang, K. Jia, Y. Liang, W. Wang, Y. Guo, H. Xia, S. Zhu *et al.*, *Laser Photonics Rev.* **2200662** (2023).
- [32] Q.-F. Yang, X. Yi, K. Y. Yang, and K. Vahala, *Nat. Photonics* **11**, 560 (2017).

- [33] See Supplemental Material at <http://link.aps.org/supplemental/10.1103/PhysRevLett.130.153802> for details of the fabrication process, theoretical models, numerical simulations, and experimental methods, which includes Refs. [34–38].
- [34] R. Y. Chiao, E. Garmire, and C. H. Townes, *Phys. Rev. Lett.* **13**, 479 (1964).
- [35] D. Korobko, I. Zolotovskii, V. Svetukhin, A. Zhukov, A. Fomin, C. Borisova, and A. Fotiadi, *Opt. Express* **28**, 4962 (2020).
- [36] E. Obrzud, S. Lecomte, and T. Herr, *Nat. Photonics* **11**, 600 (2017).
- [37] X. Yi, Q.-F. Yang, X. Zhang, K. Y. Yang, X. Li, and K. Vahala, *Nat. Commun.* **8**, 14869 (2017).
- [38] C. Deakin, Z. Zhou, and Z. Liu, *Opt. Lett.* **46**, 1345 (2021).
- [39] H. Zhou, Y. Geng, W. Cui, S.-W. Huang, Q. Zhou, K. Qiu, and C. Wei Wong, *Light* **8**, 50 (2019).
- [40] W. Loh, S. B. Papp, and S. A. Diddams, *Phys. Rev. A* **91**, 053843 (2015).
- [41] M. H. Pfeiffer, C. Herkommer, J. Liu, H. Guo, M. Karpov, E. Lucas, M. Zervas, and T. J. Kippenberg, *Optica* **4**, 684 (2017).
- [42] J. Riemensberger, A. Lukashchuk, M. Karpov, W. Weng, E. Lucas, J. Liu, and T. J. Kippenberg, *Nature (London)* **581**, 164 (2020).
- [43] M. Soriano-Amat, H. F. Martins, V. Durán, L. Costa, S. Martin-Lopez, M. Gonzalez-Herraez, and M. R. Fernández-Ruiz, *Light* **10**, 51 (2021).
- [44] Q.-F. Yang, B. Shen, H. Wang, M. Tran, Z. Zhang, K. Y. Yang, L. Wu, C. Bao, J. Bowers, A. Yariv *et al.*, *Science* **363**, 965 (2019).
- [45] B. Wang, Z. Yang, X. Zhang, and X. Yi, *Nat. Commun.* **11**, 3975 (2020).

Supplementary Material for “Soliton microcombs multiplexing using intracavity-stimulated Brillouin lasers”

Hao Zhang^{1,#}, Teng Tan^{1,#}, Hao-Jing Chen^{2,6,#}, Yan Yu^{2,6,#}, Wenting Wang^{3,#},
Bing Chang¹, Yupei Liang¹, Yanhong Guo¹, Heng Zhou¹, Handing Xia⁴, Qihuang
Gong², Chee Wei Wong³, Yunjiang Rao^{1,5,*}, Yun-Feng Xiao^{2,*}, and Baicheng Yao^{1,*}

¹*Key Laboratory of Optical Fibre Sensing and Communications (Education Ministry of China),
University of Electronic Science and Technology of China, Chengdu 611731, China.*

²*State Key Laboratory for Mesoscopic Physics and Frontiers Science Center for Nano-optoelectronics,
School of Physics, Peking University, Beijing 100871, China.*

³*Fang Lu Mesoscopic Optics and Quantum Electronics Laboratory,
University of California, Los Angeles, CA 90095, United States.*

⁴*Research Center of Laser Fusion, China Academic of Engineering Physics, Mianyang 621900, China.*

⁵*Research Centre for Optical Fiber Sensing, Zhejiang Laboratory, Hangzhou 310000, China.*

⁶*Present address: T. J. Watson Laboratory of Applied Physics,
California Institute of Technology, Pasadena, CA 91125, USA.*

(Dated: March 20, 2023)

CONTENTS

I. Fabrication of the over-modal microsphere resonator	2
II. Properties of the over-modal silica microresonator	2
III. Interactions of the pump laser, the Brillouin laser and their Kerr combs	5
IV. Generation and characterization of DKS in the over-modal microresonator	9
References	12

I. FABRICATION OF THE OVER-MODAL MICROSPHERE RESONATOR

Fig. S1(a) shows the fabrication flow and pictures of the microresonator used in our experiment. We applied arc-discharge fusing method to prepare our microresonator samples. First, we prepared silica fiber with removed coating (about 1 cm) at one end, then put it in a programmable fiber fusion splicer (FITELE S184) and fixed the end of the optical fiber a few millimeters beyond the discharge electrode. Then, we erected the fiber fusion splicer for stabilization. Finally, we ensured that the end of fiber is clean via discharging for 40 ms for removing impurities from the fiber surface and then arc-spliced the fiber for 4000 ms. After a few seconds of cooling, the microsphere resonator was fabricated. Benefiting from our programmable fiber fusion splicer, the arc discharge power, discharge duration, and discharge position were precisely controllable, and able to prepare different samples in diverse sizes. The microspheres prepared by this method can have ultrahigh Q values ($\sim 10^8$). To verify the smoothness of the surface, we utilized the scanning electron microscope (SEM) to check the microsphere resonator, as shown in Fig. S1(b). Fig. S1(c) exhibits our packaged portable dual-comb generation device, which includes a bonder, an optical fiber polarization controller and a temperature controller. The microresonator is fixed at the center of the cross-type metal bonder, which has a transverse groove to place the tapered fiber. When the coupling position of the tapered fiber and the microresonator is corrected, we fix the tapered fiber with ultraviolet glue, shut the cover of bonder and tighten it with screws.

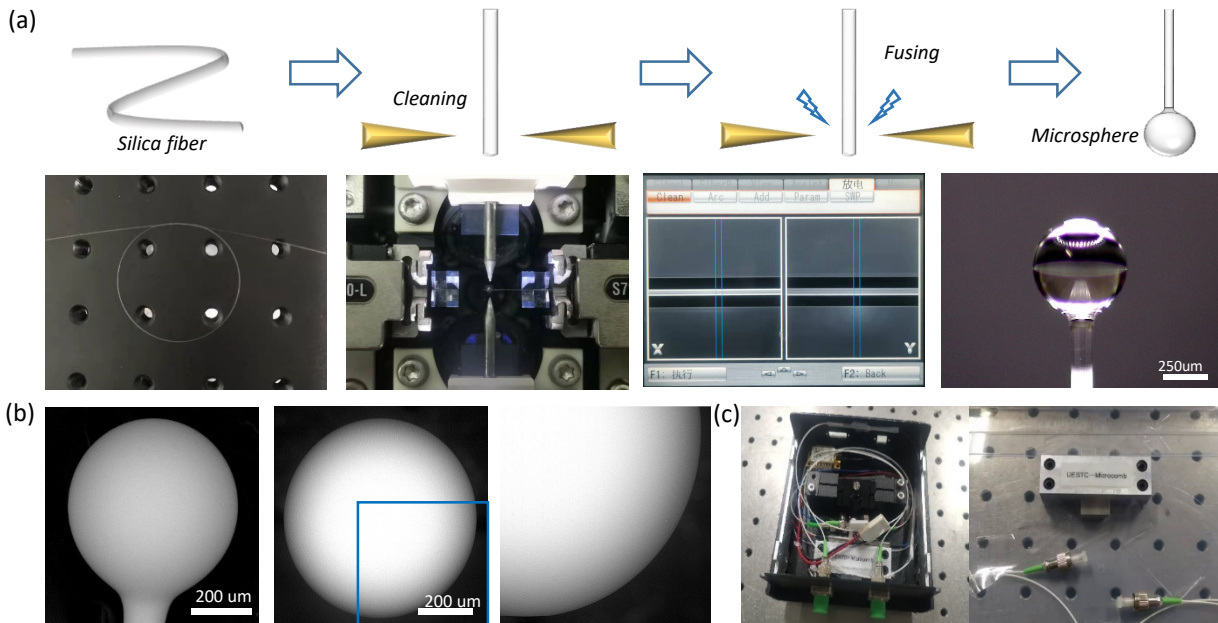


Fig. S 1: Fabrication and characterization of the microresonator. (a) Fabrication flow. (b) SEM images of the microresonator sample. (c) Images of the packaged dual-comb generation device.

II. PROPERTIES OF THE OVER-MODAL SILICA MICRORESONATOR

By using the finite element method (FEM) in a commercial software *COMSOL Multiphysics*, we simulate the mode field distribution of several typical modes in our microsphere resonator, as shown in Fig. S2(a). In this simulation, we use the following parameters: microsphere diameter 570 μm, silica material index 1.446, central wavelength 1550 nm. In this simulation, we map the normalized intensity of the electrical fields. Based on the FEM simulation, we also include the group index n_g of these modes, as Fig. S2(b) shows. From TE_{01} to TE_{05} mode, and TM_{01} to TM_{05} mode, n_g decreases with the increasing mode order. In practice, there are much more transverse mode families (for instance the dashed curves show the n_g of TE_{11} to TE_{15} and TM_{11} to TM_{15} mode), which enable very rich mode-to-mode interactions for the Brillouin laser generation and comb formation. It is clear that a higher order mode has a relatively

larger mode volume and smaller n_g . Free spectral range ($D_1/2\pi$) of a mode family is written in

$$\frac{D_1}{2\pi} = \frac{c}{n_g L} \quad (1)$$

Here L is the cavity perimeter, n_g is the group index. This suggests that for varied mode families, D_1 could be different. The repetition frequency difference between the PL- and BL-based comb is related to the group refractive index of the PL and BL mode (n_{PL} and n_{BL}) via

$$\Delta f_{\text{rep}} = \frac{\Delta D_1}{2\pi} = \frac{c}{L} |n_{\text{PL}}^{-1} - n_{\text{BL}}^{-1}| \quad (2)$$

We also note that when the dual comb repetition frequency difference is too large meanwhile the optical span of the comb is broad, RF spectral aliasing would happen, as frequency difference of the pump-Brillouin lasers is typically limited by $\Delta f_{\text{PB}} \approx 10.48$ GHz. In Fig. S2(c), we simulate the beat notes (101 lines) of dual comb with 10 MHz repetition rate difference and 330 MHz repetition rate difference respectively. Spectral coverage of the dual comb beating with $\Delta f_{\text{rep}} = 10$ MHz is 1 GHz, while spectral coverage of the dual comb beating with $\Delta f_{\text{rep}} = 330$ MHz is 33 GHz, which exceeds Δf_{PB} and causes aliasing in the RF spectrum.

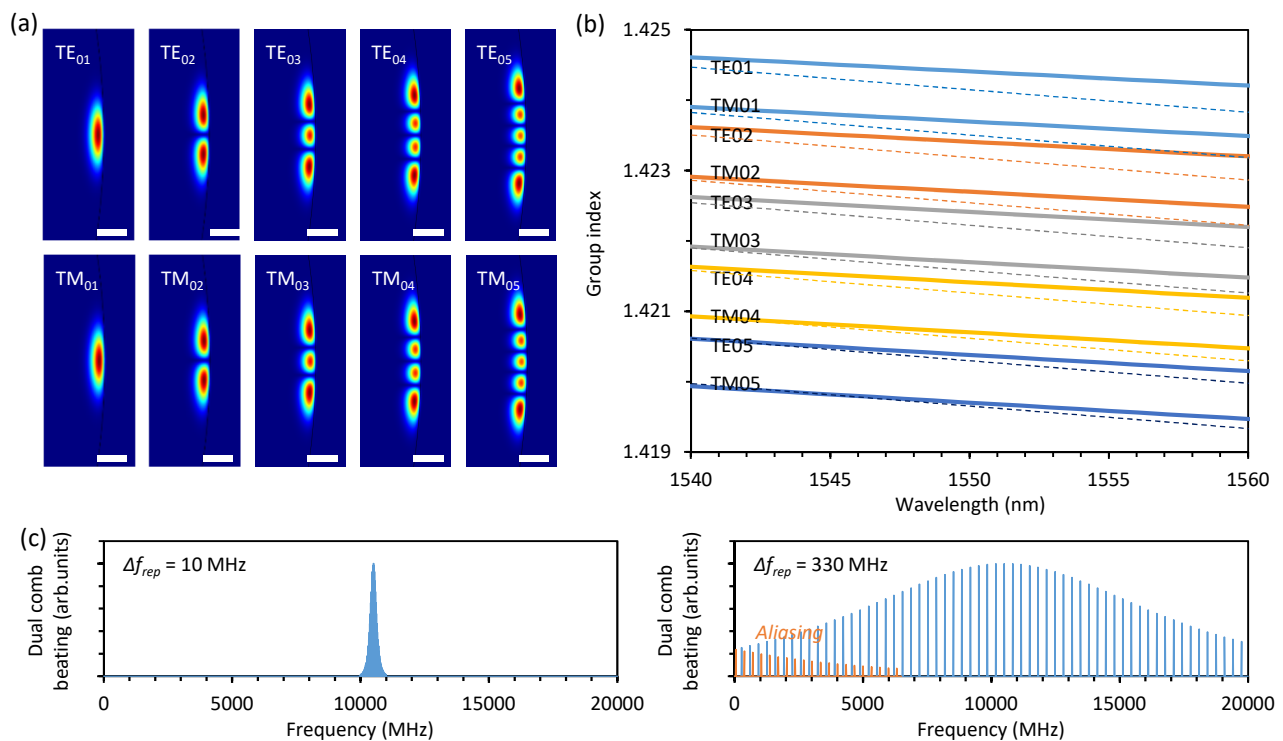


Fig. S 2: Properties of the over-modal microresonator. (a) Simulated electrical field distributions of 10 transverse modes in a silica microsphere resonator, whose diameter is 600 μm . (b) Calculated group index of different mode families. Wavelength range: 1540 nm to 1560 nm. (c) Assuming there are two dual-comb pairs with both 101 comb lines, this panel show the cases of the dual comb beats. Left panel: $\Delta f_{\text{rep}} = 10$ MHz; right panel: $\Delta f_{\text{rep}} = 330$ MHz. Each panel contains 101 beat notes.

Referring the relationship $\beta = n_g \omega / c$, and $\beta_m = d^m \beta / d\omega^m$, we numerically calculate the high order dispersions of the TE₀₁ - TE₀₄ modes in Fig. S3. Here n_g is the group index, ω is the optical frequency, c is the light velocity. One can observe that both the chromatic dispersion β_2 and the 3rd order dispersion β_3 of a higher mode order goes higher. For instance, at 1550 nm, β_2 of the TE₀₁/TM₀₁ approximately equal to -89.1 fs²/mm, while β_2 of the TE₀₄/TM₀₄ approximately equal to -93.7 fs²/mm & -92.3 fs²/mm. Meanwhile, at 1550 nm, β_3 of the TE₀₁/TM₀₁ approximately equal to 5.18 fs³/ μm , while β_3 of the TE₀₄/TM₀₄ approximately equal to 5.29 fs³/ μm & 5.25 fs³/ μm .

We measure the transmission spectrum of our over-modal microresonator, by using a tunable laser (Santec TSL-710) under 1 mW power (far below the nonlinear threshold). Fig. S4(a) plots the transmission spectrum in 5 nm

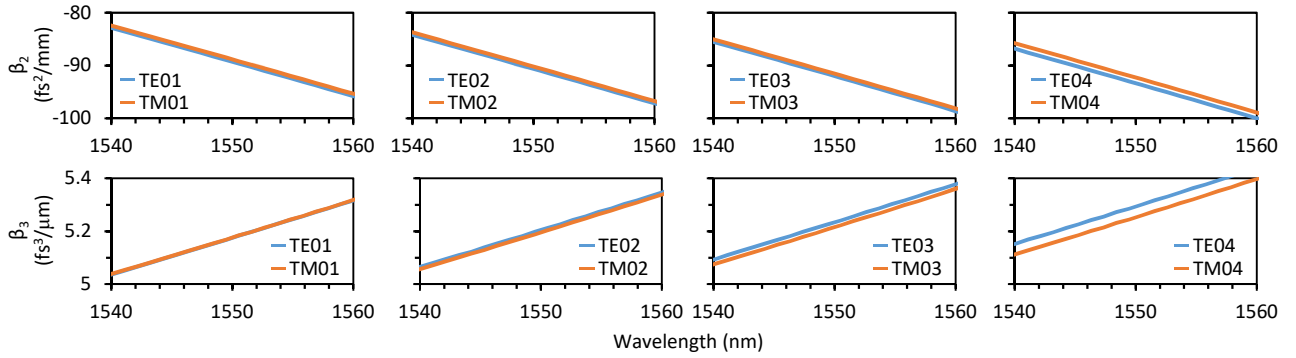


Fig. S 3: Calculated β_2 and β_3 of some mode families for example.

44 range. Here we can see the mode clusters distributed regularly in every free-spectral-range (FSR, ≈ 112 GHz). There
 45 are more than 120 resonances in each cluster. Such a high mode density provides us rich opportunities to find
 46 specific resonances for cascaded Brillouin laser excitation. In Fig. S4(b), we measure the Q factors of distinct mode
 47 families in the band 1550 nm to 1552 nm. Specifically, for the mode TE₀₁, TE₀₂, TE₀₃, and TE₁₁, Q factor decreases
 48 from 1.12×10^8 to 0.88×10^8 ; for the mode TM₀₁, TM₀₂, TM₀₃, and TM₁₁, Q factor decreases from 1.24×10^8 to
 49 0.92×10^8 . These numbers are high enough for soliton generation. Referring to the parametric oscillation threshold
 50 $P_{\text{in,th}} = \pi n_0 \omega_0 A_{\text{eff}} / 4 \eta n_2 D_1 Q^2$ (a few milliwatts under current experiment conditions), a 50 mW pump laser power is
 51 sufficient for dual-soliton formation. In the above equation, n_0 is the refractive index at the pumping frequency ω_0 ,
 52 A_{eff} is the mode area, η characterizes the bus-cavity loading, n_2 is the 3rd order nonlinear index, D_1 is 2π times the
 53 cavity FSR (equals to the comb repetition rate).

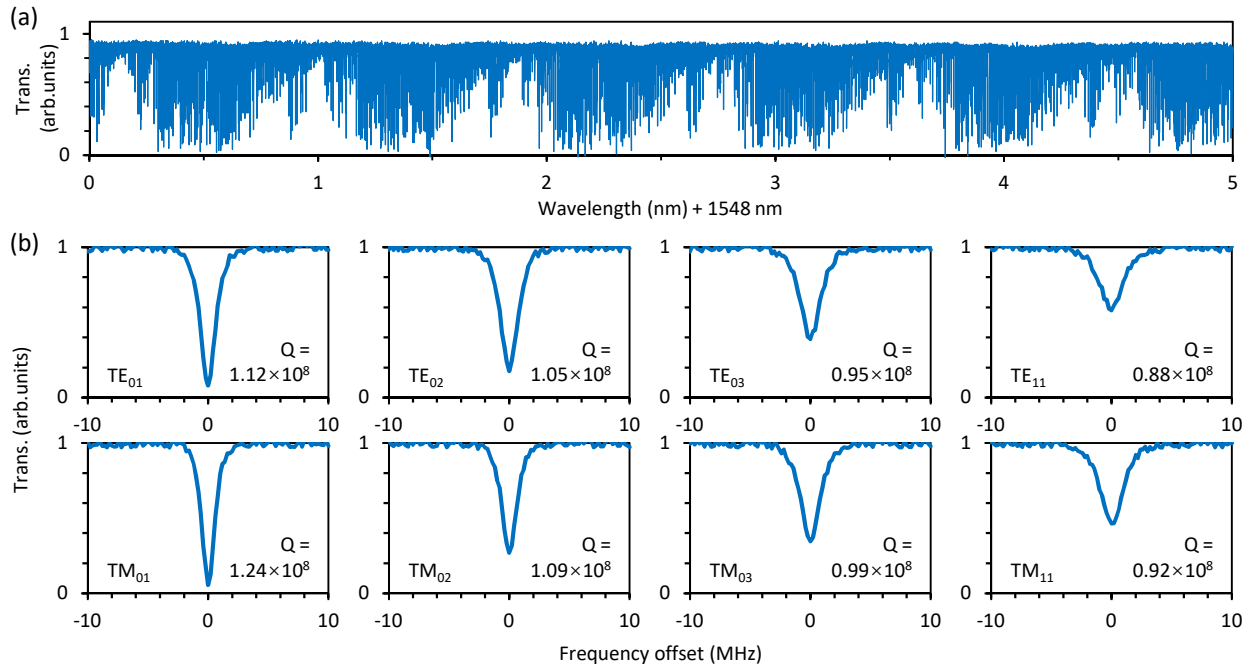


Fig. S 4: Passive transmission of the over-modal microresonator. (a) Measured transmission in the wavelength range 1548 nm to 1553 nm. (b) Measured single resonances.

54 III. INTERACTIONS OF THE PUMP LASER, THE BRILLOUIN LASER AND THEIR KERR COMBS

55 The stimulated Brillouin scattering (SBS) [1] is classically described as a nonlinear process between the pumping
 56 wave and the Stokes wave via acoustic interaction, which modulates the media index effectively. In quantum optics,
 57 this process is also regarded as the annihilation of a pump photon with the generation of a Stokes photon and an
 58 acoustic phonon. Phase matching condition of the SBL is $\Omega_A = \omega_p - \omega_s$, $\mathbf{k}_A = \mathbf{k}_p - \mathbf{k}_s$. Here Ω_A , ω_p , ω_s are the
 59 acoustic frequency, pump frequency, Stokes frequency, while \mathbf{k}_A , \mathbf{k}_p , \mathbf{k}_s are wavevectors of the acoustic wave, pump
 60 wave, and Stokes wave respectively. Ω_A and \mathbf{k}_A are related by $\Omega_A = v_A |\mathbf{k}_A|$, where $v_A \approx 5.7$ km/s is the velocity of the
 61 acoustic wave in silica. As $v_A \ll c$, Brillouin laser can only be generated in the opposite (backward) direction of the
 62 pump laser, meaning that $|\mathbf{k}_A| = |\mathbf{k}_p| + |\mathbf{k}_s| \approx 2|\mathbf{k}_p|$ and therefore $\Omega_A \approx 2v_A |\mathbf{k}_p| \approx 2\pi \times 10.5$ GHz. Typically in silica,
 63 the Brillouin gain bandwidth is narrow, on a level of several MHz, comparable to the resonance linewidth. Therefore,
 64 Brillouin lasing happens when there is a high Q resonance within the gain bandwidth, and the lasing frequency lies
 65 between the center frequency of the resonance and the gain peak. Here in our high Q over-modal silica microresonator,
 66 both SBS and Kerr nonlinearity are present, which are responsible for Brillouin lasing and microcomb generation,
 67 respectively. To investigate the process of counter-propagating dual-comb formation, a set of coupled mode equations
 68 incorporating the dynamics of the forward, backward, and acoustic (density) wave fields is introduced (see [2] and
 69 Ref [40] in maintext, where only Brillouin scattering is present):

$$\begin{aligned}
 \frac{dA_\mu}{dt} &= - \left[\frac{\gamma_A}{2} + i(\omega_{\mu A} - \omega_{0A} - \mu D_{1A}) \right] A_\mu + i \frac{\gamma_e \omega_{0A}}{4n_0^2 \rho_0} K B_0 \rho \delta_{\mu 0} \\
 &\quad + ig_{K,AA} \sum_{\mu_1, \mu_2} A_{\mu_1} A_{\mu_2} A_{\mu_1 + \mu_2 - \mu}^* + 2ig_{K,AB} \sum_{\mu_1} |B_{\mu_1}|^2 A_\mu + F \exp[-i(\omega_{PL} - \omega_{0A})t] \delta_{\mu 0} \\
 \frac{dB_\mu}{dt} &= - \left[\frac{\gamma_B}{2} + i(\omega_{\mu B} - \omega_{0B} - \mu D_{1B}) \right] B_\mu + i \frac{\gamma_e \omega_{0B}}{4n_0^2 \rho_0} K A_0 \rho^* \delta_{\mu 0} \\
 &\quad + ig_{K,BB} \sum_{\mu_1, \mu_2} B_{\mu_1} B_{\mu_2} B_{\mu_1 + \mu_2 - \mu}^* + 2ig_{K,AB} \sum_{\mu_1} |A_{\mu_1}|^2 B_\mu \\
 \frac{d\rho}{dt} &= - \left(\frac{\Gamma}{2} + i \frac{\Omega_b^2 - \Omega^2}{2\Omega} \right) \rho + i \frac{\varepsilon_0 \gamma_e}{4\Omega} \frac{l_\rho^2}{R^2} K A_0 B_0^*
 \end{aligned} \tag{3}$$

70 where A_μ and B_μ are the slowly varying field amplitude of the μ th mode in the forward (c.c.w.) and backward (c.w.)
 71 direction referenced to the frequencies $\omega_{0A} + \mu D_{1A}$ and $\omega_{0B} + \mu D_{1B}$ respectively, with $\omega_{\mu A(B)}$ the resonance frequency
 72 of the μ th mode, and $D_{1A(B)}/2\pi$ the FSR of the respective mode family. Note that $\mu = 0$ denotes the pump mode
 73 in the forward direction and the Brillouin lasing mode in backward direction, and the resonance frequencies can be
 74 described by the parabolic dispersion: $\omega_{\mu A(B)} = \omega_{0A(B)} + D_{1A(B)}\mu + D_{2A(B)}\mu^2/2$, where $D_{2A(B)}$ denotes the second
 75 order dispersion. ρ is the amplitude of the acoustic wave referenced to $\Omega = \omega_{0A} - \omega_{0B}$. γ_A , γ_B , and Γ are the loss
 76 rate of the optical and acoustic modes, Ω_b is the central Brillouin frequency shift, γ_e is the electrostriction coefficient,
 77 n_0 is the refractive index, ρ_0 is the material (silica) density, and K represents the overlap of the forward, backward,
 78 and acoustic waves. $l_\rho = l_A + l_B$ is the angular momentum of the acoustic wave, R denotes the resonator radius, and
 79 $\delta_{\mu 0}$ is the Kronecker delta function. $g_{K,AA(BB)}$ and $g_{K,AB}$ are the Kerr self- and cross-phase modulation coefficients,
 80 ω_{PL} is the pump laser frequency, and F is the pumping term (taken as a positive real value).

81 The above equation set does not yield a steady-state solution for the field amplitudes, as the fields A_μ , B_μ , and
 82 ρ are not referenced to their real oscillation frequencies $\omega_{PL} + \mu D_{1A}$, $\omega_{BL} + \mu D_{1B}$, and Ω_ρ , where ω_{BL} (Ω_ρ) is the
 83 frequency of the Brillouin laser (density wave), with $\omega_{PL} - \omega_{BL} = \Omega_\rho$. This problem can be remedied by defining

$$\begin{aligned}
 A'_\mu &= A_\mu e^{-i\sigma_A t} \\
 B'_\mu &= B_\mu e^{-i\sigma_B t} \\
 \rho' &= \rho e^{-i\sigma_\rho t}
 \end{aligned} \tag{4}$$

84 where $\sigma_A = \omega_{0A} - \omega_{PL}$, $\sigma_B = \omega_{0B} - \omega_{BL}$, and $\sigma_\rho = \Omega - \Omega_\rho$, with $\sigma_A = \sigma_B + \sigma_\rho$. The coupled equations then transforms

85 into

$$\begin{aligned}
\frac{dA'_\mu}{dt} &= - \left[\frac{\gamma_A}{2} + i(\omega_{\mu A} - \omega_{PL} - \mu D_{1A}) \right] A'_\mu + i \frac{\gamma_e \omega_{0A}}{4n_0^2 \rho_0} K B'_0 \rho' \delta_{\mu 0} \\
&\quad + i g_{K,AA} \sum_{\mu_1, \mu_2} A'_{\mu_1} A'_{\mu_2} A'^*_{\mu_1 + \mu_2 - \mu} + 2i g_{K,AB} \sum_{\mu_1} |B'_{\mu_1}|^2 A'_\mu + F \delta_{\mu 0} \\
\frac{dB'_\mu}{dt} &= - \left[\frac{\gamma_B}{2} + i(\omega_{\mu B} - \omega_{BL} - \mu D_{1B}) \right] B'_\mu + i \frac{\gamma_e \omega_{0B}}{4n_0^2 \rho_0} K A'_0 \rho'^* \delta_{\mu 0} \\
&\quad + i g_{K,BB} \sum_{\mu_1, \mu_2} B'_{\mu_1} B'_{\mu_2} B'^*_{\mu_1 + \mu_2 - \mu} + 2i g_{K,AB} \sum_{\mu_1} |A'_{\mu_1}|^2 B'_\mu \\
\frac{d\rho'}{dt} &= - \left[\frac{\Gamma}{2} + i \left(\frac{\Omega_b^2 - \Omega^2}{2\Omega} + \sigma_\rho \right) \right] \rho' + i \frac{\varepsilon_0 \gamma_e}{4\Omega} \frac{l_\rho^2}{R^2} K A'_0 B_0'^*
\end{aligned} \tag{5}$$

86 Other than the trivial solution $B'_\mu = 0$, $\rho' = 0$, there exists another solution for the amplitude and frequency of the
87 optical waves and the acoustic wave, which should be our focus here.

88 While it is impossible to solve the coupled equation set analytically for the entire soliton generation process (e.g.,
89 the chaotic MI comb is not even a steady state), we focus on several points of importance, namely the onset of
90 Brillouin lasing and comb generation. Without loss of generality, we obtain the nontrivial steady state solution prior
91 to the BL-based comb generation, with the assumption that the forward field also reaches a steady state

$$\begin{aligned}
\sigma_B &= \frac{\gamma_B}{\gamma_B + \Gamma} \left(\sigma_A + \frac{\Omega_b^2 - \Omega^2}{2\Omega} \right) + \frac{\Gamma}{\gamma_B + \Gamma} \left(g_{K,BB} |B'_0|^2 + 2g_{K,AB} \sum_{\mu_1} |A'_{\mu_1}|^2 \right) \\
\sigma_\rho &= \frac{\Gamma}{\gamma_B + \Gamma} \left(\sigma_A - g_{K,BB} |B'_0|^2 - 2g_{K,AB} \sum_{\mu_1} |A'_{\mu_1}|^2 \right) - \frac{\gamma_B}{\gamma_B + \Gamma} \frac{\Omega_b^2 - \Omega^2}{2\Omega} \\
\tan(\phi_{A0} - \phi_{B0} - \phi_\rho) &= - \frac{\gamma_B + \Gamma}{2 \left[\sigma_A - g_{K,BB} |B'_0|^2 - 2g_{K,AB} \sum_{\mu_1} |A'_{\mu_1}|^2 + (\Omega_b^2 - \Omega^2)/2\Omega \right]} \\
|A'_0|^2 &= \frac{4n_0^2 \rho_0 \Gamma \gamma_B \Omega R^2}{\varepsilon_0 \gamma_e^2 \omega_{0B} l_\rho^2 K^2} \sin^{-2}(\phi_{A0} - \phi_{B0} - \phi_\rho) \\
|B'_0|^2 &= \frac{1}{\gamma_B} \left[2F |A'_0| \cos(\phi_{A0}) - \gamma_A \sum_{\mu_1} |A'_{\mu_1}|^2 \right] \\
|\rho'| &= - \frac{\varepsilon_0 \gamma_e l_\rho^2 K}{2\Gamma \Omega R^2} |A'_0| |B'_0| \sin(\phi_{A0} - \phi_{B0} - \phi_\rho)
\end{aligned} \tag{6}$$

92 Note that $|B'_0|^2 \geq 0$ is required for the nontrivial solution to be meaningful (a threshold condition for SBS), otherwise
93 the system would be in the trivial steady state. Here ϕ_{A0} , ϕ_{B0} , and ϕ_ρ are the argument of A'_0 , B'_0 , and ρ' respectively,
94 and $(\phi_{A0} - \phi_{B0} - \phi_\rho) = -\pi/2$ (or equivalently $\sigma_A - g_{K,BB} |B'_0|^2 - 2g_{K,AB} \sum_{\mu_1} |A'_{\mu_1}|^2 + (\Omega_b^2 - \Omega^2)/2\Omega = 0$) represents
95 optimal phase matching for SBS. According to Eq. S6, Brillouin lasing requires good phase matching, otherwise $|A'_0|^2$
96 would be large, which may result in a negative $|B'_0|^2$. Note that the frequency of the Brillouin laser and the optimal
97 phase matching condition can expressed as

$$\begin{aligned}
\omega_{BL} &= \frac{\Gamma}{\gamma_B + \Gamma} \left(\omega_{0B} - g_{K,BB} |B'_0|^2 - 2g_{K,AB} \sum_{\mu_1} |A'_{\mu_1}|^2 \right) + \frac{\gamma_B}{\gamma_B + \Gamma} (\omega_{PL} - \Omega_b) \\
\omega_{0B} - g_{K,BB} |B'_0|^2 - 2g_{K,AB} \sum_{\mu_1} |A'_{\mu_1}|^2 &= \omega_{PL} - \Omega_b
\end{aligned} \tag{7}$$

98 where $|\Omega_b - \Omega| \ll \Omega$ is assumed so that $(\Omega_b^2 - \Omega^2)/2\Omega \approx \Omega_b - \Omega$. The terms in the two brackets represent frequency of
99 the Kerr-effect-shifted resonance and the peak of Brillouin gain spectrum, respectively. When they are equal, optimal
100 phase matching is achieved.

101 The above coupled equation set is derived in the frequency domain and can be transformed into the time domain[3]:

$$\begin{aligned}
\frac{\partial A'}{\partial t} &= -\left(\frac{\gamma_A}{2} + i\sigma_A\right) A' + i\frac{D_{2A}}{2} \frac{\partial^2 A'}{\partial \phi^2} + ig_{K,AA}|A'|^2 A' + 2ig_{K,AB} \left(\int_0^{2\pi} |B'|^2 \frac{d\phi}{2\pi}\right) A' + i\frac{\gamma_e \omega_{0A}}{4n_0^2 \rho_0} K B'_0 \rho' + F \\
\frac{\partial B'}{\partial t} &= -\left(\frac{\gamma_B}{2} + i\sigma_B\right) B' + i\frac{D_{2B}}{2} \frac{\partial^2 B'}{\partial \phi^2} + ig_{K,BB}|B'|^2 B' + 2ig_{K,AB} \left(\int_0^{2\pi} |A'|^2 \frac{d\phi}{2\pi}\right) B' + i\frac{\gamma_e \omega_{0B}}{4n_0^2 \rho_0} K A'_0 \rho'^* \\
\frac{d\rho'}{dt} &= -\left[\frac{\Gamma}{2} + i\left(\frac{\Omega_b^2 - \Omega^2}{2\Omega} + \sigma_\rho\right)\right] \rho' + i\frac{\varepsilon_0 \gamma_e}{4\Omega} \frac{l_\rho^2}{R^2} K A'_0 B_0'^*
\end{aligned} \tag{8}$$

102 where $A' = \sum_\mu A'_\mu \exp(i\mu\phi)$ and $B' = \sum_\mu B'_\mu \exp(i\mu\phi)$. Note that A' and B' are in electric field units, and ρ' is in
103 the unit of density. To facilitate numerical simulations, we rewrite the time domain dynamical equations to resemble
104 the Lugiato-Lefever equation (LLE)

$$\begin{aligned}
\frac{\partial \tilde{A}}{\partial t} &= -\left(\frac{\gamma_A}{2} + i\sigma_A\right) \tilde{A} + i\frac{D_{2A}}{2} \frac{\partial^2 \tilde{A}}{\partial \phi^2} + i\tilde{g}_{K,AA}|\tilde{A}|^2 \tilde{A} + 2i\tilde{g}_{K,AB} \left(\int_0^{2\pi} |\tilde{B}|^2 \frac{d\phi}{2\pi}\right) \tilde{A} + i\tilde{B}_0 \tilde{\rho} + \tilde{F} \\
\frac{\partial \tilde{B}}{\partial t} &= -\left(\frac{\gamma_B}{2} + i\sigma_B\right) \tilde{B} + i\frac{D_{2B}}{2} \frac{\partial^2 \tilde{B}}{\partial \phi^2} + i\tilde{g}_{K,BB}|\tilde{B}|^2 \tilde{B} + 2i\tilde{g}_{K,AB} \left(\int_0^{2\pi} |\tilde{A}|^2 \frac{d\phi}{2\pi}\right) \tilde{B} + i\tilde{A}_0 \tilde{\rho}^* \\
\frac{d\tilde{\rho}}{dt} &= -\left[\frac{\Gamma}{2} + i\left(\frac{\Omega_b^2 - \Omega^2}{2\Omega} + \sigma_\rho\right)\right] \tilde{\rho} + i\frac{\hbar\omega_0^2 \gamma_e^2 l_\rho^2 K^2}{8n_0^4 \rho_0 \Omega R^2 V_{AB}} \tilde{A}_0 \tilde{B}_0^*
\end{aligned} \tag{9}$$

105 Here, $\tilde{A} = \sum_\mu \tilde{A}_\mu \exp(i\mu\phi)$ and $\tilde{B} = \sum_\mu \tilde{B}_\mu \exp(i\mu\phi)$, where $|\tilde{A}_\mu|^2$ and $|\tilde{B}_\mu|^2$ denote the photon number in the μ th
106 mode, $\tilde{\rho}$ is in the unit of s^{-1} , $\tilde{g}_{K,ij} = \hbar\omega_0^2 n_2 c/n_0^2 V_{ij}$, where V_{ij} is the optical mode volume and cross mode volume
107 for $(i,j) = (A,B)$, and $\tilde{F} = \sqrt{\gamma_{ex} P_{in}/\hbar\omega_0}$, where γ_{ex} is the coupling loss rate and P_{in} is the pump power. Using the
108 above equations, we numerically calculate the dual-soliton solution, as shown in Fig. S5. The parameters used in the
109 simulation are $\omega_0/2\pi = 193$ THz, $\gamma_A/2\pi = 1.93$ MHz, $\gamma_B/2\pi = 2.58$ MHz, $\Gamma/2\pi = 7.74$ MHz, $(\Omega_b^2 - \Omega^2)/2\Omega = 14.5$
110 MHz, $\tilde{g}_{K,AA} = \tilde{g}_{K,BB} = 2\tilde{g}_{K,AB} = 3.0 \times 10^{-3} s^{-1}$, $n_0 = 1.45$, $\gamma_e = 1.5$, $\rho_0 = 2200$ kg/m³, $R = 300\mu m$, $\Omega/2\pi = 10.48$
111 GHz, and $K = 0.5$.

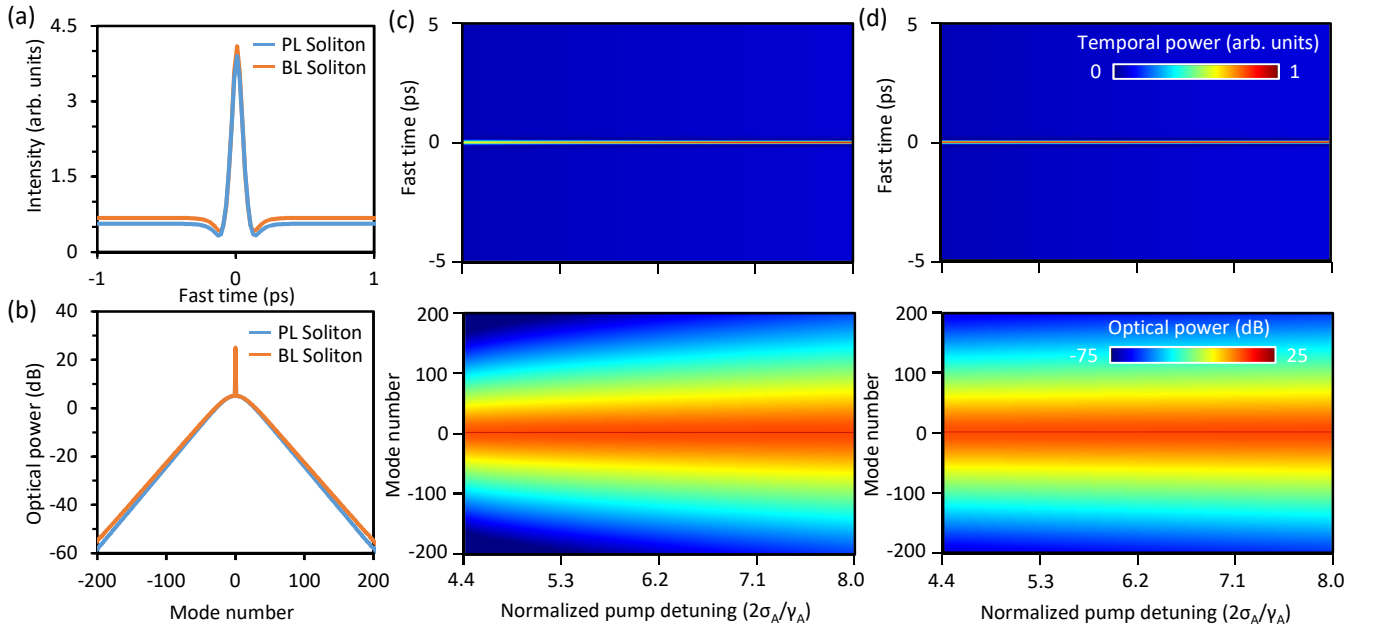


Fig. S 5: Simulation of dual-soliton coexistence. (a) Temporal waveform of PL and BL soliton at normalized detuning $2\sigma_A/\gamma_A = 6.9$. (b) Dual-soliton spectra at the same detuning. (c),(d) Evolution of PL and BL soliton when increasing the pump laser detuning adiabatically. Top panel maps the temporal evolution; bottom maps the spectral evolution.

Next we analyze the noise performance of the dual-comb beat note. First, we consider the factors influencing the repetition rate difference between the pump laser based soliton and the Brillouin laser based soliton $\Delta\omega_{\text{rep}} = |\omega_{\text{rep,PL}} - \omega_{\text{rep,BL}}|$ and its noise performance. Note that the soliton repetition rate does not necessarily equal to the FSR, as other effects like Raman interactions and dispersive waves may alter the repetition rate [4]. In experiment, the repetition rate difference between the dual-comb pair is mainly determined by the FSR difference (Eq. S2), as no obvious dispersive waves and Raman induced spectral red-shifts are observed in the measured optical spectra. Nevertheless, both the Raman and dispersive wave interactions can convert fluctuations in laser detuning into the noise of the comb repetition rate. As the FSR is dependent on the group refractive index, which is then related to the cavity temperature (controlled by a thermoelectric cooler in experiment), a thermal fluctuation would induce noise in the repetition rate signal. Such a thermal noise is strongly suppressed in the $\Delta\omega_{\text{rep}}$ signal, because it is mainly a common mode noise for the PL and BL mode and is canceled out in $\Delta\omega_{\text{rep}}$. For the PL- and BL-based soliton comb, the phase noise of the n th comb line is given by:

$$\begin{aligned}\Delta\varphi_{\text{PL},n}(t) &= \Delta\varphi_{\text{PL}}(t) + n\Delta\varphi_{\text{rep,PL}}(t) \\ \Delta\varphi_{\text{BL},n}(t) &= \Delta\varphi_{\text{BL}}(t) + n\Delta\varphi_{\text{rep,BL}}(t)\end{aligned}\quad (10)$$

where $\Delta\varphi_{\text{rep,PL}}$ and $\Delta\varphi_{\text{rep,BL}}$ are phase fluctuations in the repetition rates, and $\Delta\varphi_{\text{PL}}$ and $\Delta\varphi_{\text{BL}}$ are inherent noise of the lasers. Since the Brillouin laser is generated by the pump, $\Delta\varphi_{\text{PL}}$ and $\Delta\varphi_{\text{BL}}$ could be almost cancelled (limited by the acoustic mode Q factor) at the coherent receiver during the dual-comb beating process when the optical path difference between the two combs is significantly shorter than the coherence length [5]. The total phase noise of the n th comb line in the dual-comb beat note is:

$$S_n(f) = S_{\Delta f_{\text{PB}}}(f) + n^2 S_{\Delta f_{\text{rep}}}(f) \quad (11)$$

where $S_{\Delta f_{\text{PB}}}(f)$ and $S_{\Delta f_{\text{rep}}}(f)$ are phase noise of the PL-BL beat note and the repetition rate difference.

Experimentally, we measure the correlation of pump laser frequency and the Brillouin laser frequency using an optical spectrometer. Fig. S6(a) plots the optical spectrum in range of 1549.5 nm to 1550.5 nm, inside one can see both the pump laser and the Brillouin laser. The blue curve plots the original state, where two solitons have already been generated by the pump laser and the Brillouin laser respectively. Then we further red-tune the pump wavelength, as the orange and the grey curve shows. Specifically, when the pump laser wavelength shifts from 1549.998 nm to 1550.01 nm and 1550.034 nm, the Brillouin laser shifts from 1550.088 nm to 1550.094 nm and 1550.105 nm. In Fig. S6(b), we summarize this linear correlation, which agrees with the theoretical trend (Eq. S7). By red-tuning the pump laser wavelength 0.036 nm (≈ 4.5 GHz), red-shift of the Brillouin laser is only 0.017 nm (≈ 2.1 GHz).

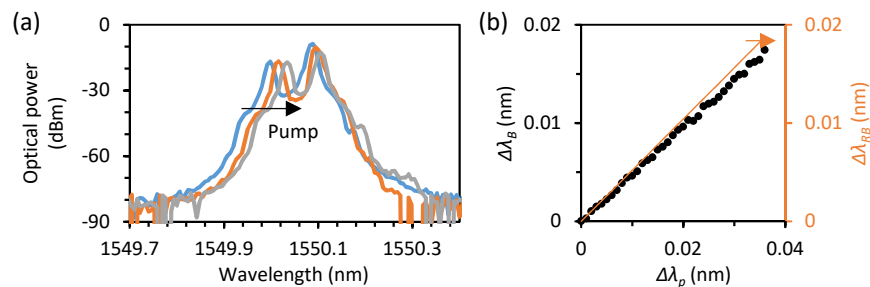


Fig. S 6: Measured red-detuning of the Brillouin laser corresponding to the pump laser. (a) Local spectra containing the pump laser and the Brillouin laser, initially they are already in the red-detuning region of their resonances. (b) Black dots: Correlation of the wavelength shifts between the pump laser and the Brillouin laser. Orange curve: estimated shift of the resonance where the Brillouin laser is located at.

In experiment, the over-modal nature of our microsphere provides a possibility that cascaded Brillouin lasers can be generated, when the cascaded Brillouin gain regions overlap with more than one resonances. Fig. S7(a) shows the measured Brillouin gain band of a section of the silica fiber (we use it for the microsphere fabrication). This gain band is measured under a pump power below lasing threshold. The measured Brillouin frequency conversion is $\Delta f_{\text{PB}} \approx 10.46$ GHz, with a gain bandwidth $\Delta G \approx 62$ MHz. When we want to generate a Brillouin laser, it is essential to ensure that a resonance can be included in the Brillouin gain band. Note that the above two parameters (Δf_{PB} and ΔG) are fixed by the material. In Fig. S7(b), we plot the transmission spectrum of our microcavity (193.5 THz

145 ~ 193.55 THz, or 1549.99 nm ~ 1550.49 nm). In this range, we can find chances to generate $0 \sim 4$ Brillouin lasers
 146 deterministically. For instance, Fig. S7(c) shows 2 detailed examples (case i : no BL can be generated, case ii : 4
 147 BLs can be generated). In case i , there is no resonance within the Brillouin gain band ~ 10.46 GHz below the pump
 148 mode. In case ii , 4 cascaded Brillouin gain regions overlap with 4 resonances.

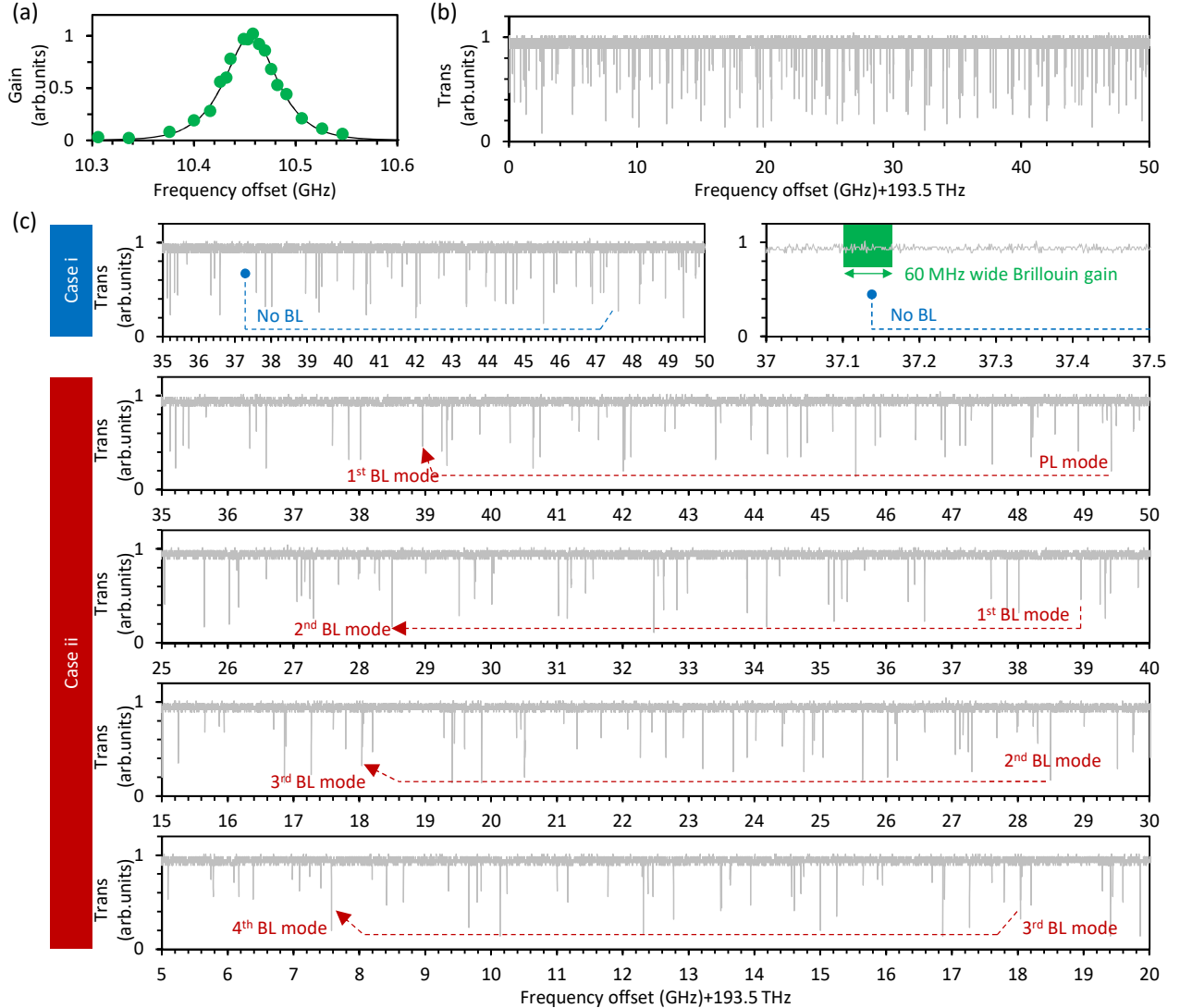


Fig. S 7: Principle and deterministic generation of cascaded Brillouin lasers. (a) Brillouin gain region in the silica fiber, which is used in the microcavity fabrication. Green dots: measured data, black curve: Lorentz fitting. (b) Transmission of our microcavity, in the band 193.5 to 193.55 THz. (c) For two different pumping mode, two cases that cascaded Brillouin lasers cannot and can be generated.

149 IV. GENERATION AND CHARACTERIZATION OF DKS IN THE OVER-MODAL MICRORESONATOR

150 Fig. S8(a) shows our experimental setup for comb generation. First a tunable ECDL (external cavity diode
 151 laser, Santec TSL-710, typical linewidth 200 kHz, tunable range 1480 \sim 1640 nm) is used to as the pump laser.
 152 The tunable ECDL is amplified by using a high power / low noise EDFA (erbium doped fiber amplifier, Max-ray
 153 photonics, EYDFA-HP-C-BA-30-B) through a FPC (fiber polarization controller) and then launched into a tapered
 154 fiber (diameter ≈ 1 μ m), for the bus-cavity coupling. We use a TEC (thermal electrical cooler, Thorlabs TC-200) to
 155 accurately control the temperature, with resolution 10 mK. Between the microresonator and the FPC, we insert a

156 circulator to measure the comb propagated backwardly. The generated combs are measured in OSA (optical spectrum
 157 analyzer, Yokogawa 6370D) and ESA (electrical spectrum analyzer, R&S 0 ~ 43 GHz). For obtaining better comb
 158 stability, we also use NKT Koheras BASIK E15 (with 1.5 nm tunable bandwidth around 1550 nm) as the pumping
 159 laser.

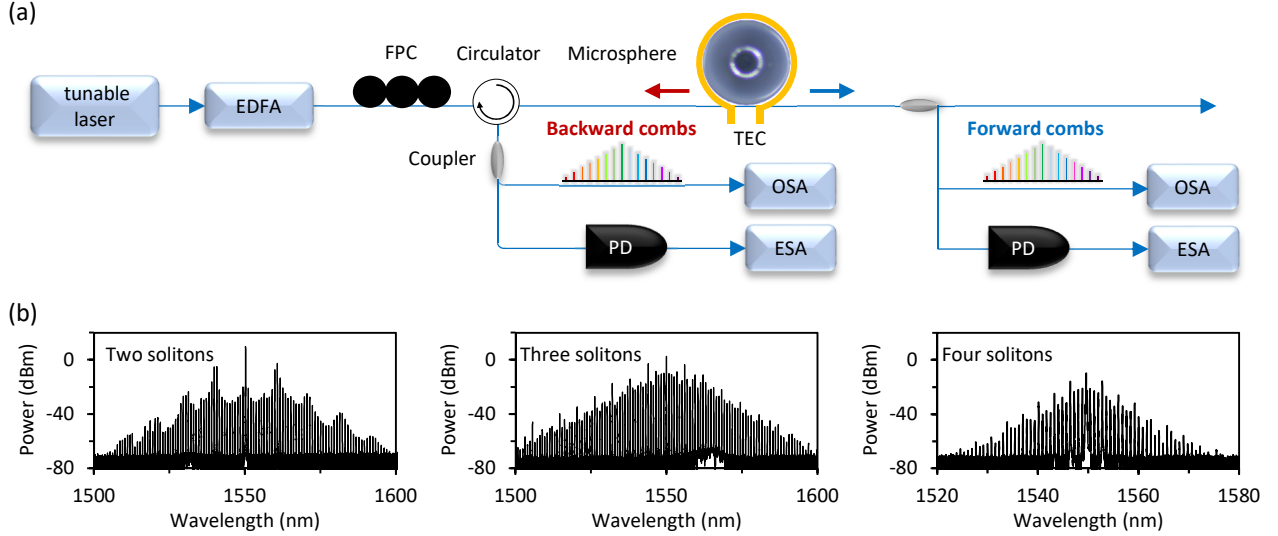


Fig. S 8: Generating the DKSs. (a) Experimental setup. EDFA: erbium doped fiber amplifier, FPC: fiber polarization controller, PD: photonic detector, OSA: optical spectrum analyzer, ESA: electrical spectrum analyzer. (b) Spectral examples. Besides single soliton, other soliton states such as 2-4 solitons per roundtrip are also observable.

160 In experiment, besides the single soliton state, there also appears multi soliton states, in both forward and backward
 161 direction, determined by the laser detuning. Fig. S8(b) plots the spectra of several multi soliton states for instance.
 162 From left to right, we demonstrate a two-soliton state, a three-soliton state and a four-soliton state. All these states
 163 have low intensity noise in the RF domain.

164 In Fig. S9, we show the scheme to measure the linewidths and relative intensity noises of the pump / Brillouin
 165 laser, and the comb lines. First, Fig. S9(a) demonstrates the experimental setup for the heterodyne measurement.
 166 By filtering the forward and backward propagating laser line and comb line, we measure the linewidth and noise of
 167 the pump laser driven DKS and the Brillouin laser driven DKS respectively. Specifically, a wavelength selectable
 168 switcher (WSS, WSS- Santec wss-1000) is used to filter out the laser line or a single comb line of the DKS. Then a
 169 1:9 coupler divides the line into two propagating paths. The 90% part of the signal passes through a fiber optic delay
 170 line (~50km), and the other is modulated by the acoustic-optical modulator (AOM, AOM-GOOCH & HOUSEGO
 171 T-M080-0.4C2J-3-F2P) with a frequency shift of 80MHz. Finally, the two signals are coupled back and detected in a
 172 photodetector, thus we obtain the heterodyne frequency spectrum after auto-correlation release.

173 Fig. S9(b) plots the laser linewidth of our Santec TSL-710, and the first comb line (single soliton state) excited
 174 by this laser instrument. Linewidth of the TSL-710 at ≈ 1550 nm is 230 kHz, correspondingly linewidth of the first
 175 single comb line at ≈ 1551 nm (single soliton state) is 242 kHz. Fig. S9(c) plots the case when we change the Santec
 176 TSL-710 (widely tunable laser) to the NKT Koheras BASIK E15 (low noise single-frequency laser with < 200 GHz
 177 tunable band). Linewidth of the NKT-E15 at ≈ 1550 nm is 110 Hz, correspondingly linewidth of the first single
 178 comb line at ≈ 1551 nm (single soliton state) is 140 Hz. Fig. S9(d) and (e) plots the relative intensity noises (RINs)
 179 when we use the two different laser instruments. RIN is obtained by using an electrical spectrum analyzer and an
 180 oscilloscope (1.25 GHz band width, 4 GHz sampling rate). In the electrical spectrum analyzer (with an appropriate
 181 resolution bandwidth, RBW), we get the noise of photodetector ($P_0(f)$) under the condition of empty-load. Then,
 182 we measure the signal of DKS in the photodetector, and the voltage average value of the signal ($E[x(t)]$) is obtained by
 183 an oscilloscope with the fixed loading resistance $R_L = 50\Omega$. Finally, we obtain the power spectral density of the signal
 184 ($P_{\text{integrating}}(f)$) from the spectrum analyzer with the same RBW. The RIN of the signal is calculated according to
 185 the formula:

$$\text{RIN} = \frac{N}{A} = \frac{(P_{\text{integrating}}(f) - P_0(f))/\text{RBW}}{E[x(t)]^2/R_L} \quad (12)$$

186 In these two panels, we see RIN of the DKS line obeys the characteristics from the pump laser. When we use the
 187 TSL-710, RIN is about -84 dB/Hz at 1 Hz offset while about -136 dB/Hz at 10 kHz offset. When we use the NKT
 188 E-15, RIN is about -105 dB/Hz at 1 Hz offset while about -139 dB/Hz at 10 kHz offset.

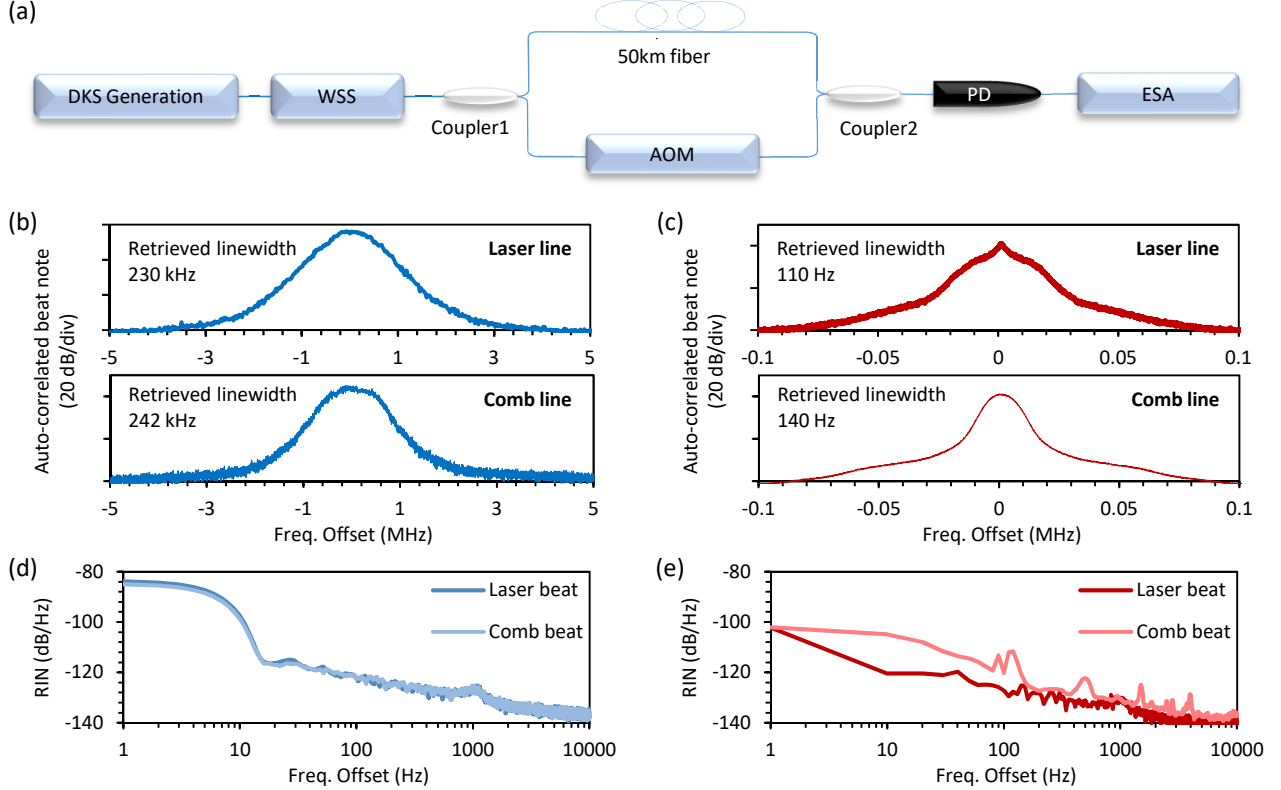


Fig. S 9: Performance of the pump lasers and their driven DKSs. (a) Experimental setup for optical linewidth measurement. WSS: wavelength selective switch, AOM: acousto-optic modulator, PD: Photodetector, ESA: electrical spectrum analyzer. (b) Heterodyne self-beating note of the pump laser (TSL-710) and its first comb line. (c) Heterodyne self-beating note of the pump laser (NKT E-15) and its first comb line. (d) Relative intensity noise (RIN) of the pump laser (TSL-710) and its first comb line. (e) Relative intensity noise (RIN) of the pump laser (NKT E-15) and its first comb line.

189 As shown in Fig. 2, we obtain an electrical comb in the RF domain using a photodetector, by combining two solitons
 190 together. Here we discuss the phase noises. There are two important beating signals, one is the Pump-Brillouin offset,
 191 $\Delta f_{\text{PB}} = 10.4802$ GHz, and the other one is the interval between the electrical comb lines, $\Delta f_{\text{rep}} = 8.5$ MHz. Fig.
 192 S10(a) shows the two beat notes specifically, signal to noise ratio (SNR) of both the two beating lines are higher than
 193 60 dB. Fig. S10(b) plots the single-sideband phase noise (SSB-PN) of the them. Specifically, for the Δf_{PB} beat note,
 194 we obtain the phase noise reaches -130 dBc/Hz at 1 MHz offset, comparable to the microwave synthesizer using an
 195 on-chip Brillouin oscillator, Ref [26] in maintext. For the Δf_{rep} beat note, the phase noise approaches -120 dBc/Hz
 196 at 1 kHz offset, and -154 dBc/Hz at 1 MHz offset. The low noise of the Δf_{rep} beating line benefits from the ‘single
 197 cavity + single pump’ scheme. We also note that noise of the Δf_{rep} is essentially different from the optical noise of the
 198 f_{rep} in other reports using just one cavity. In our scheme, since the BL is generated by the PL, noise from the lasers’
 199 fluctuation is correlative and canceled after coherent receiving. Besides, since the two soliton combs are generated
 200 in one single cavity, the detuning-based common mode noise and differential mode noise are avoided, meanwhile the
 201 opto-thermal noise related to the cavity is also effectively suppressed. Fig. S10(c) plots the measured frequency noise
 202 of the PL. Thanks to the high Q cavity, white noise limited linewidth of the PL reaches 6.02 Hz, this number is about
 203 3-folds better than the state-of-the-art Brillouin laser generation using a microdisk resonator, Ref [28] in maintext.

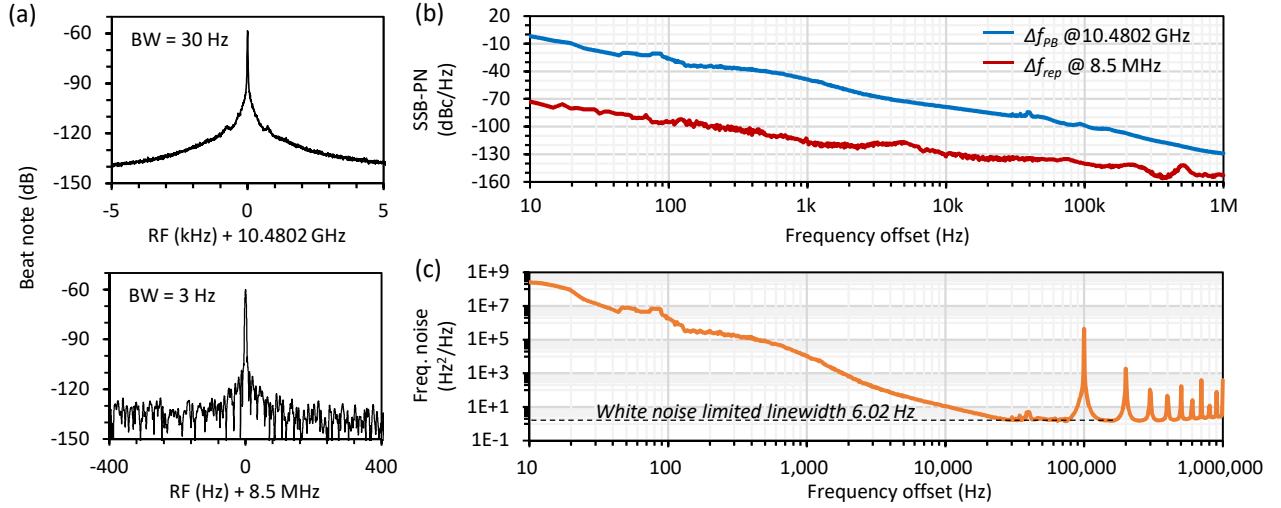


Fig. S 10: RF analysis. (a) Measured RF of the Δf_{PB} beat note and the Δf_{rep} beat note in high resolution. (b) Measured single-sideband phase noises of the Δf_{PB} beat note (blue) and the Δf_{rep} beat note (red). (c) Frequency noise of the Brillouin laser.

-
- 204 [1] R. Y. Chiao, E. Garmire, and C. H. Townes, Physical review letters **13**, 479 (1964).
 205 [2] D. Korobko, I. Zolotovskii, V. Svetukhin, A. Zhukov, A. Fomin, C. Borisova, and A. Fotiadi, Optics Express **28**, 4962
 206 (2020).
 207 [3] E. Obrzud, S. Lecomte, and T. Herr, Nature Photonics **11**, 600 (2017).
 208 [4] X. Yi, Q.-F. Yang, X. Zhang, K. Y. Yang, X. Li, and K. Vahala, Nature communications **8**, 1 (2017).
 209 [5] C. Deakin, Z. Zhou, and Z. Liu, Optics Letters **46**, 1345 (2021).